Anal. Chem. **2009,** *81,* 716–724

Characterizing Metabolic Inhibition Using Electrochemical Enzyme/DNA Biosensors

Dominic O. Hull,[†] Besnik Bajrami,[†] Ingela Jansson,[‡] John B. Schenkman,[‡] and James F. Rusling*[,†,‡]

Department of Chemistry and Institute of Materials Science, University of Connecticut, 55 N. Eagleville Road, Storrs, Connecticut 06269, and Department of Cell Biology, University of Connecticut Health Center, Farmington, Connecticut 06032

Studies of metabolic enzyme inhibition are necessary in drug development and toxicity investigations as potential tools to limit or prevent appearance of deleterious metabolites formed, for example, by cytochrome (cyt) P450 enzymes. In this paper, we evaluate the use of enzyme/DNA toxicity biosensors as tools to investigate enzyme inhibition. We have examined DNA damage due to cyt P450cam metabolism of styrene using DNA/enzyme films on pyrolytic graphite (PG) electrodes monitored via Ru(bpy)$_3^{2+}$-mediated DNA oxidation. Styrene metabolism initiated by hydrogen peroxide was evaluated with and without the inhibitors, imidazole, imidazole-4-acetic acid, and sulconazole (in micromolar range) to monitor DNA damage inhibition. The initial rates of DNA damage decreased with increased inhibitor concentrations. Linear and nonlinear fits of Michaelis−Menten inhibition models were used to determine apparent inhibition constants (K_I*) for the inhibitors. Elucidation of the best fitting inhibition model was achieved by comparing correlation coefficients and the sum of the square of the errors (SSE) from each inhibition model. Results confirmed the utility of the enzyme/DNA biosensor for metabolic inhibition studies. A simple competitive inhibition model best approximated the data for imidazole, imidazole-4-acetic acid and sulconazole with K_I* of 268.2, 142.3, and 204.2 μM, respectively.

Metabolic enzymes catalyze the formation of more soluble metabolites from lipophilic foreign molecules to assist with clearance from the body.[1−4] However, these enzymes can also bioactivate molecules to reactive metabolites that react with DNA, proteins, and other biomolecules.[5−7] Inhibition of enzyme activity by ingested molecules or drugs can cause serious toxicity problems by allowing concentrations of co-metabolized substances to reach dangerous levels. This is well-known in the pharmaceutical industry in which these so-called *drug-drug interactions* (DDI) can adversely influence the concentrations or biological action of other administered drugs.[8−12] These interactions are either inhibition or induction of drug metabolism which can lead to either increased drug concentration (inhibitory) or reduced drug levels (induction) in the body.[9] The cytochrome P450 (CYP) enzymes are responsible for ~75% of oxidative xenobiotic metabolism and are especially important for DDI.[8,11,13] Understanding the levels of DDI typically requires measuring the inhibition constant (K_I) and the rate of drug metabolism.[14,15]

We have developed electrochemical biosensors featuring films containing cyt P450s and DNA to screen metabolic bioactivation and genotoxicity of xenobiotic compounds and drugs.[16−33] The required films can be made on single pyrolytic graphite electrodes

* To whom correspondence should be addressed. E-mail: james.rusling@uconn.edu.

[†] University of Connecticut.

[‡] Department of Cell Biology, University of Connecticut Health Center.

(1) Bjorkman, S. *Clin. Pharmacokinet.* **2006**, *45*, 1–11.
(2) Klotz, U. *Clin. Pharmacokinet.* **2007**, *46*, 985–996.
(3) Pang, K. S.; Gillette, J. R. *J. Pharmacol. Exp. Ther.* **1978**, *207*, 178–194.
(4) Shitara, Y.; Sato, H.; Sugiyama, Y. *Annu. Rev. Pharmacol. Toxicol.* **2005**, *45*, 689–723.
(5) *Enzymatic Basis of Detoxification*; Jacoby, W. B., Ed.; Academic Press: New York, 1980; Vols. *I* and *II*.
(6) Rooney, P. H.; Telfer, C.; McFadyen, M. C. E.; Melvin, W. T.; Murray, G. I. *Curr. Cancer Drug Targets* **2004**, *4*, 257–265.
(7) Schenkman, J. B.; Greim, H. *Cytochrome P450*; Springer Verlag: Berlin, 1993.
(8) Lee, M. D.; Ayanoglu, E.; Gong, L. *Xenobiotica* **2006**, *36*, 1013–1080.
(9) Leucuta, S. E.; Vlase, L. *Curr. Clin. Pharm.* **2006**, *1*, 5–20.
(10) Obach, R. S.; Walsky, R. L.; Venkatakrishnan, K.; Houston, J. B.; Tremaine, L. M. *Clin. Pharmacol. Ther.* **2005**, *78*, 582–592.
(11) Venkatakrishnan, K.; Obach, R. S.; A., R.-H. *Xenobiotica* **2007**, *37*, 1225–1256.
(12) Zhang, Z.-Y.; Wong, Y. N. *Curr. Drug Metab.* **2005**, *6*, 241–257.
(13) Brown, H. S.; Ito, K.; Galetin, A.; Houston, J. B. *Br. J. Clin. Pharmacol.* **2005**, *60*, 508–518.
(14) Brown, H. S.; Chadwick, A.; Houston, J. B. *Drug Metab. Dispos.* **2007**, *35*, 2119–2126.
(15) Rochat, B. *Clin. Pharmacokinet.* **2005**, *44*, 349–366.
(16) Bajrami, B.; Hvastkovs, E. G.; Jensen, G. C.; Schenkman, J. B.; Rusling, J. F. *Anal. Chem.* **2008**, *80*, 922–932.
(17) Dennany, L.; Forster, R. J.; Rusling, J. F. *J. Am. Chem. Soc.* **2003**, *125*, 5213–5218.
(18) Dennany, L.; Forster, R. J.; White, B.; Smyth, M.; Rusling, J. F. *J. Am. Chem. Soc.* **2004**, *126*, 8835–8841.
(19) Estavillo, C.; Lu, Z. Q.; Jansson, I.; Schenkman, J. B.; Rusling, J. F. *Biophys. Chem.* **2003**, *104*, 291–296.
(20) Hvastkovs, E. G.; So, M.; Krishnan, S.; Bajrami, B.; Tarun, M.; Jansson, I.; Schenkman, J. B.; Rusling, J. F. *Anal. Chem.* **2007**, *79*, 1897–1906.
(21) Mugweru, A.; Rusling, J. *Electroanalysis* **2006**, *18*, 327–332.
(22) Munge, B.; Estavillo, C.; Schenkman, J. B.; Rusling, J. F. *ChemBioChem* **2003**, *4*, 82–89.
(23) Rusling, J. F.; Hvastkovs, E. G.; Hull, D. O.; Schenkman, J. B. *Chem. Commun.* **2008**, 141–154.
(24) So, M.; Hvastkovs, E. G.; Bajrami, B.; Schenkman, J. B.; Rusling, J. F. *Anal. Chem.* **2008**, *80*, 1192–1200.
(25) So, M.; Hvastkovs, E. G.; Schenkman, J. B.; Rusling, J. F. *Biosens. Bioelectron.* **2007**, *23*, 492–498.
(26) Tarun, M.; Bajrami, B.; Rusling, J. F. *Anal. Chem.* **2006**, *78*, 624–627.
(27) Tarun, M.; Rusling, J. F. *Anal. Chem.* **2005**, *77*, 2056–2062.

10.1021/ac802179s CCC: $40.75
Published on Web 12/18/2008

(PG),[17−19,21−25,28,29] in a PG block array format,[20,30] or on silica nanoparticles for product generation and LC-MS analysis.[16,32] Studies conducted on these various biosensor formats include the metabolism and genotoxicity of styrene,[17,19,22,27−29] benzo[a]pyrene,[20] *N*-nitrosamines,[16,30] and the genotoxicity of arylamines as activated by *N*-acetyltransferase.[24,31] In addition to formation of reactive metabolites and genotoxicity, the enzyme/DNA biosensors have been developed to examine tandem metabolism by phase I (Cytochrome P450 1A2) and phase II (*N*-acetyltransferase) enzymes,[31] to study the inhibitory effects of antioxidants on procarcinogenic metabolism,[21] and to determine IC_{50} values for the competitive inhibition of *N*-nitrosamine metabolism with rat liver microsomes by competitive inhibitors of CYP3A4 and CYP2E1.[32]

We have previously shown that antioxidants afforded protection of DNA in our biosensor by scavenging reactive oxygen species (ROS). The antioxidants employed (flavinoids and Vitamin C) were effective at the active site of the enzyme in films reducing the generation of ROS's.[21] However, those experiments did not yield any mechanistic data on the mode of inhibition beyond demonstrating decrease in DNA damage signals by antioxidants.

In this paper, we evaluate enzyme/DNA biosensors to measure enzyme inhibition constants and inhibition kinetics on a model system. The sensor contained bacterial cyt P450cam (CYP101) DNA, and the test substrate, styrene. Styrene was chosen as the model substrate because of its metabolism by cyt P450cam and metabolite genotoxicity toward guanine nucleobases in DNA.[19,22,26−29,34−36] Herein, we followed inhibitory effects of imidazoles by measuring the level of DNA damage from the styrene metabolite, styrene oxide. The imidazoles exert inhibitory effects by direct coordination with the heme iron via the N3 position on the imidazole ring and/or by acting as an antioxidant (Scheme 1).[37−46] Using ruthenium tris(2−2′ bipyridine) [$Ru(bpy)_3^{2+}$] as the electrochemical catalyst for DNA oxidation,[47−49] we monitored changes in the sensor signals in the presence of inhibitors. Styrene oxide−guanine adducts in DNA cause localized bulges in the DNA allowing closer approach of $Ru(bpy)_3^{2+}$ which facilitates electrocatalytic detection.[28,29,49] Therefore, DNA is the mode by which signals arise from our biosensor, and it is thereby sensitive to changes in the amounts of genotoxic metabolites that cause the damage. Changes in initial rates of DNA damage because of cytochrome P450cam conversion of styrene to styrene oxide as a function of inhibitor concentrations are evaluated and used as the basis for the determination of inhibition constants. Data were evaluated using Michaelis−Menten models to obtain inhibition parameters. The inhibition constants are directly related to the sensor action and indicate the changes in substrate metabolism or DNA adduct formation in the presence of the inhibitor.

Scheme 1. Structures of Imidazole Inhibitors Used in Inhibition Studies[a]

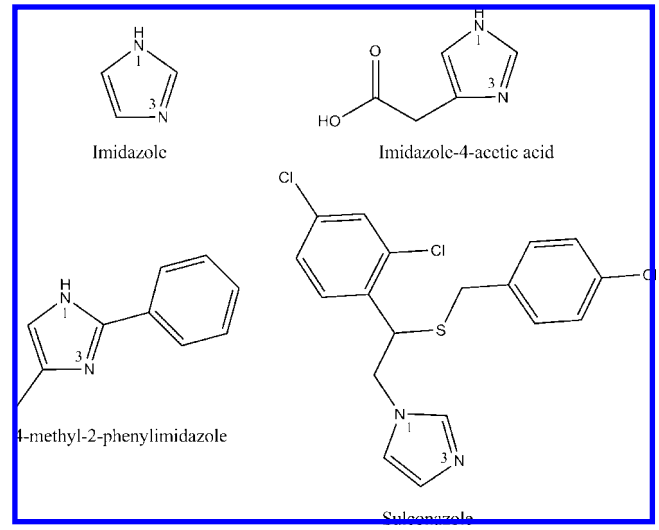

[a] Labeled is the N3 position that is integral part of imidazole/cytochrome P450 binding.

EXPERIMENTAL SECTION

Chemicals and Materials. Tris(2,2′-bipyridyl)dichloro-ruthenium(II) hexahydrate $Ru(bpy)_3Cl_2$, double stranded salmon testes DNA (st-DNA), poly(diallydimethylammonium-chloride) (PDDA, MW < 200,000), imidazole, imidazole-4-acetate sodium salt, sulconazole nitrate, 4-methyl-2-phenyl-imidazole, styrene, and dimethylsulfoxide (DMSO) where obtained from Sigma-Aldrich. All other chemicals were reagent grade. Water was purified with a Hydro Nanopure system with specific resistance >16 MΩ cm. Cytochrome P450cam (CYP101, MW 46,500), was expressed in *Escherichia coli* DH5α clone J5 followed by isolation and purification. The method developed by Omura and Sato[50] was used to determine enzyme concentration.

(28) Zhou, L. P.; Rusling, J. F. *Anal. Chem.* **2001**, *73*, 4780–4786.
(29) Zhou, L. P.; Yang, J.; Estavillo, C.; Stuart, J. D.; Schenkman, J. B.; Rusling, J. F. *J. Am. Chem. Soc.* **2003**, *125*, 1431–1436.
(30) Krishnan, S.; Hvastkovs, E. G.; Bajrami, B.; Jansson, I.; Schenkman, J. B.; Rusling, J. F. *Chem. Commun.* **2007**, 1713–1715.
(31) So, M.; Schenkman, J. B.; Rusling, J. F. *Chem. Commun.* **2008**, in press.
(32) Bajrami, B.; Krishnan, S.; Rusling, J. F. *Drug Metab. Lett.* **2008**, *2* (3), 158–162.
(33) Krishnan, S.; Hvastkovs, E. G.; Bajrami, B.; Choudhary, D.; Schenkman, J. B.; Rusling, J. F. *Anal. Chem.* **2008**, *80*, 5279–5285.
(34) Nickerson, D. P.; Harford-Cross, C. F.; Fulcher, S. R.; Wong, L.-L. *FEBS Lett.* **1997**, *405*, 153–156.
(35) Fruetel, J. A.; Collins, J. R.; Camper, D. L.; Loew, G. H.; Ortiz de Montellano, P. R. *J. Am. Chem. Soc.* **1992**, *114*, 6987–6993.
(36) Fruetel, J. A.; Mackman, R. L.; Peterson, J. A.; Ortiz de Montellano, P. R. *J. Biol. Chem.* **1994**, *269*, 28815–28821.
(37) Verras, A.; Kuntz, I. D.; Ortiz de Montellano, P. R. *J. Med. Chem.* **2004**, *47*, 3572–3579.
(38) Verras, A.; Ortiz de Montellano, P. R. *Biochem. Soc. Trans.* **2006**, *34*, 1–3.
(39) Locuson, C. W.; Hutzler, J. M.; Tracy, T. S. *Drug Metab. Dispos.* **2007**, *35*, 614–622.
(40) Verras, A.; Alian, A.; Ortiz de Montellano, P. R. *Protein Eng., Des. Sel.* **2006**, *19*, 491–496.
(41) Franklin, M. R.; Constance, J. E. *Drug Metab. Rev.* **2007**, *39*, 309–322.
(42) Rogerson, T. D.; Wilkins, C. F.; Hetarski, K. *Biochem. Pharmacol.* **1977**, *26*, 1039–1042.
(43) Babizhayev, M. A.; Seguin, M.-C.; Gueyna, J.; Evstigneeva, R. P.; Ageyeva, E.; Zheltukhina, G. A. *Biochem. J.* **1994**, *304*, 509–516.
(44) Kohen, R.; Yamamoto, Y.; Cundy, K. C.; Ames, D. N. *Proc. Natl. Acad. Sci. U.S.A.* **1988**, *85*, 3175–3179.
(45) La Mendola, D.; Sortino, S.; Vecchio, G.; Rizzarelli, E. *Helv. Chim. Acta* **2002**, *85*, 1633–1643.
(46) Sorrenti, V.; Salerno, L.; Di Giacomo, C.; Acquaviva, R.; Siracusa, M. A.; Vanella, A. *Nitric Oxide* **2006**, *14*, 45–50.
(47) Rusling, J. F. *Biosens. Bioelectron.* **2004**, *20*, 1022–1028.
(48) Thorp, H. H. Long-Range Charge Transfer in DNA II. In *Topics In Current Chemistry*; Schuster, G. B., Ed.; Springer Verlag: Heidelberg, 2004; Vol. 237.
(49) Johnston, D. H.; Glasgow, K. C.; Thorp, H. H. *J. Am. Chem. Soc.* **1995**, *117*, 8933–8938.
(50) Omura, T.; Sato, R. *J. Biol. Chem.* **1964**, *239*, 2379–2385.

Experimental Analysis. The (PDDA/DNA/CYP101/)$_2$PDDA/DNA films were assembled on PG electrodes in a procedure described in earlier literature.[28,29,51,52] Quartz crystal microbalance (QCM) measurements were used to validate film formation and determine amounts of DNA and cyt P450cam as previously reported.[51,52] The DNA/CYP101 LBL films were incubated in a similar method as previously published with the exception of stirring the incubation solutions at ~300 rpm during experiments and addition of inhibitors.[21,28,29] **Safety note***: Styrene and its metabolites are suspected carcinogens. All procedures were done while wearing gloves and under closed hoods.* Square wave voltammetry was conducted with CH instrument potentiostats in analogous method as illustrated in the literature with the caveat of 10 Hz frequency and 50 mM NaH_2PO_4 pH 7.0/ 50 mM NaCl.[21,28,29] Liquid chromatography experiments with 2% styrene, 500 μM inhibitors, and cyt P450cam in biocollodal films were conducted in a similar fashion as previously reported.[16]

Michaelis−Menten constant (K_m) Determination.[53] Using the LBL-enzyme/DNA electrochemical sensor an apparent Michaelis−Menten constant (K_m*) was determined for styrene. The electrochemical signal observed for styrene oxide DNA damage was observed as function of % styrene from 0−1min. Initial rates of DNA damage signal as a function of % styrene were obtained from the slopes of the ratio of damage signal to undamaged signal (Ip_F/Ip_I) versus incubation time (Ip_F/Ip_I vs min). The percent styrene was varied from 0.05−2%. The percent styrene in the incubation cells was converted to dispersion concentration using the density of styrene and applied in the Michaelis−Menten equation. A plot of the initial rate of DNA damage versus styrene concentration was used to determine an apparent K_m and V_m (maximal velocity (rate)) by employing the nonlinear (1) and linear (2) forms of the Michaelis−Menten equation.[53]

$$v_o = \frac{V_{max} * S}{K_m + S} \tag{1}$$

$$\frac{1}{v_o} = \frac{K_m}{V_{max} * S} + \frac{1}{V_{max}} \tag{2}$$

Michaelis−Menten Inhibition Kinetics. [53]Using the LBL-enzyme/DNA electrochemical sensor, relative initial rates as a function of inhibitor concentrations were used to determine the inhibition constant. The initial rates at each inhibitor concentration (I) were obtained from plots of the ratio of damage signals to undamaged signals versus time ((Ip_F/Ip_I) vs min). The plots generated were fitted using the various Michaelis−Menten inhibition models in Kaleidagraph (Synergy Software) to determine the apparent inhibition constant (K_I*). The inhibition models include competitive (3), uncompetitive (4), and noncompetitive (5). In addition to those standard Michaelis−Menten inhibition models, a simple competitive inhibition model (6)[54] based only on the equilibrium of enzyme and the inhibitor and the competitive model that has been rearranged by $1/K_m$ (7) were employed. [55] Fittings were conducted with the previously estimated values of apparent K_m and V_m. The equations used to estimate K_I are shown below.

$$v_o = \frac{V_{max} * S}{K_m + \left({}^{(K_m * I)}/_{K_I}\right) + S} \tag{3}$$

$$v_o = \frac{V_{max} * S}{K_m + S + \left({}^{S * I}/_{K_I'}\right)} \tag{4}$$

$$v_o = \frac{V_{max} * S}{K_m + \left({}^{(K_m * I)}/_{K_I}\right) + S + \left({}^{S * I}/_{K_I'}\right)} \tag{5}$$

$$v_o = \frac{V_{max}}{1 + \frac{I}{K_I}} + \frac{V_1 * \left({}^{I}/_{K_I}\right)}{1 + \frac{I}{K_I}} \tag{6}$$

$$v_o = \frac{{}^{(V_{max} * S)}/_{K_m}}{1 + \frac{I}{K_I} + \frac{S}{K_m}} \tag{7}$$

The unknowns in the equations above are as follows; v_o is initial rate, V_{max} is the maximal velocity (rate), S is the substrate concentration, I is the inhibitor concentration, K_m is the Michaelis constant, K_I is the inhibition constant, and V_1 is the maximal velocity (rate) due to the enzyme−inhibitor state.

Regression Analysis.[54] Application of a goodness of fit error analysis was used to validate the Michaelis−Menten inhibition constant. The correlation coefficients obtained from fits were used as the initial goodness of fit criteria, followed by an analysis of a sum of the squares of the errors (SSE) to ascertain the inhibition model and constant. SSE analysis is a calculation of the sum of squared difference between measured and calculated values using the estimated parameters. The SSE values for each fitting method are compared, with the lowest SSE being indicative of the best fit. The equation for SSE (8) is as follows;

$$\mathrm{SSE}(m1) = \sum_n \left(Y_{\mathrm{Meas.}} - Y_{\mathrm{Calc.}}(x_n, \mathrm{m1})\right)^2 \tag{8}$$

For SSE, $Y_{\mathrm{Meas.}}$ is the measured value, and $Y_{\mathrm{Calc.}}(x_n,\mathrm{m1})$ is the calculated value from the appropriate expression as a function of a given x and fitted value m1.

RESULTS

Detection of DNA Damage. We previously used enzyme/DNA sensors to detect damage of DNA caused by the cyt P450cam metabolite, styrene oxide.[19,22,28,29] Briefly, films were incubated with styrene, and the enzyme was activated by 1 mM hydrogen peroxide. After incubation, sensors were rinsed and then

(51) Lvov, Y. M.; Lu, Z.; Schenkman, J. B.; Zu, X.; Rusling, J. F. *J. Am. Chem. Soc.* **1998**, *120*, 4073–4080.

(52) Lvov, Y. M. Nanostructured Materials, Micelles and Colloids. In *Handbook of Surfaces and Interfaces of Materials*; Nalwa, H. S., Ed.; Academic Press: New York, 2001; Vol. 3.

(53) Voet, D.; Voet, J. G.; Pratt, C. W. *Fundamentals of Biochemistry*; John Wiley and Sons, Inc.: New York, 1999.

(54) Rusling, J. F.; Kumosinski, T. In *Nonlinear Computer Modeling of Chemical and Biochemical Data*; Academic Press: New York, 1996.

(55) Guto, P. M.; Rusling, J. F. *J. Phys. Chem. B* **2005**, *109*, 24457–24464.

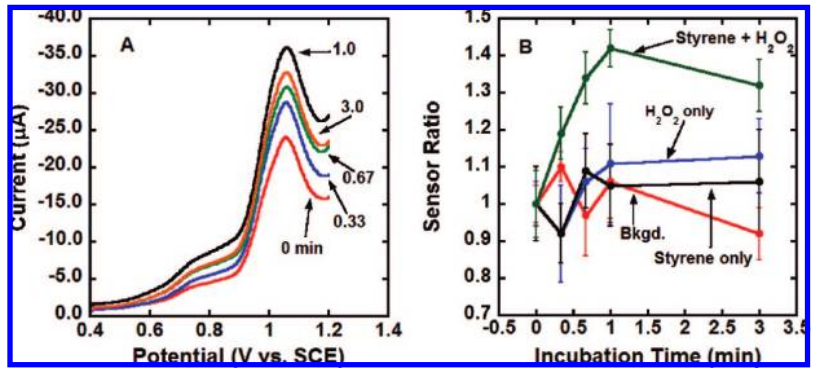

Figure 1. Square wave voltammetry (SWV) of (PDDA/DNA/CYP101/)$_2$-PDDA/DNA films in 50 mM NaH_2PO_4 pH 7.0/50 mM NaCl with 50 μM $Ru(bpy)_3Cl_2$ as the mediator. Incubations were conducted in 10 mM sodium acetate pH 5.5/50 mM NaCl at 37 °C with and without 2% styrene and 1 mM H_2O_2. (A) SWV at various incubation times. (B) Sensor Ratios (Ip_F/Ip_I) between background (no incubation) and at each incubation time. SWV parameters; amplitude 25 mV, frequency 10 Hz and step 4 mV.

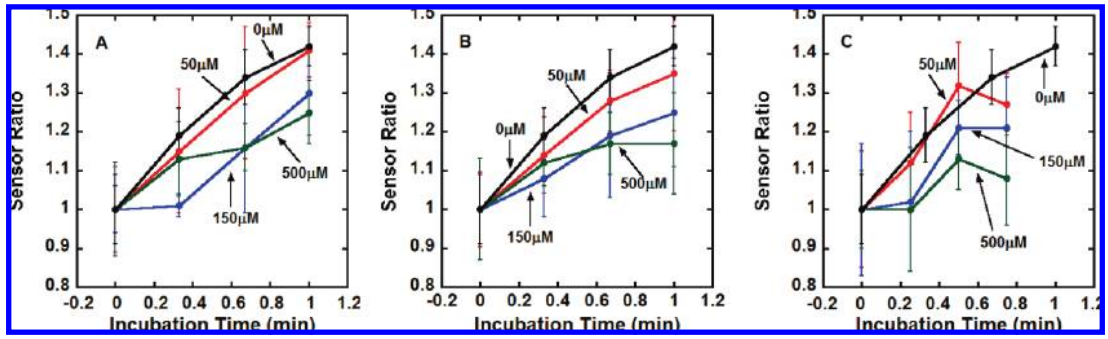

Figure 2. Sensor ratios (Ip_F/Ip_I) determined from SWV with increasing inhibitor concentrations. Incubations were conducted in 10 mM sodium acetate pH 5.5/50 mM NaCl at 37 °C with and without 2% styrene and 1 mM H_2O_2 and inhibitor. For clarity, sensor ratios for 100 μM and 250 μM inhibitor concentrations were removed from the above plots. (A) Imidazole, (B) Imidazole-4-acetic acid, and (C) Sulconazole.

probed by square wave voltammetry (SWV). We employed the $Ru(bpy)_3^{2+}$-mediated electrocatalytic oxidation of DNA as diagnostic of DNA damage.[47−49] Upon formation of styrene oxide DNA adducts, localized bulges in the DNA helix allow closer access to additional guanines yielding faster oxidation and larger electrocatalytic signals for damaged DNA. As shown in Figure 1A, the SWV electrocatalytic signal increases with increased incubation time with styrene and hydrogen peroxide up to 1 min. The signals leveled off above 1 min because of steady state styrene oxide DNA damage indicating no further increase in DNA damage with incubation time. To better illustrate the signal increase, the ratio of peak currents (Ip_F, X min) after incubation and background peak currents (Ip_I, 0 min) versus incubation time were generated. The plot of the sensor ratios (Ip_F/Ip_I) versus incubation time is shown in Figure 1B with increasing signals up to 1 min. This change was characteristic of the relative increase in DNA damage.[23,47] From the initial slope of sensor ratio versus time, a relative rate for DNA damage of 0.142 ± 0.013 min^{-1} was estimated.

Inhibition of DNA Damage. Inhibition experiments were done in a similar fashion as described for styrene metabolism except for the addition of inhibitors. Sensors featuring DNA and cyt P450cam were incubated with styrene, hydrogen peroxide, and a specific inhibitor concentration. After the period of incubation, with imidazole, imidazole-4-acetic acid or sulconazole, sensors were rinsed in water and analyzed by SWV to evaluate the extent of inhibition. The sensor ratio plots for imidazole, imidazole-4-acetic acid, and sulconazole (Figure 2) decreased with increasing inhibitor concentration, signifying the inhibition of styrene oxide-mediated DNA damage by the imidazole inhibitors. Control experiments using only inhibitors indicated no contribution of the inhibitor to the electrochemical signal (Supporting Information, Figure S6). Additionally, control experiments with 4-methyl-2-phenylimidazole in the presence of styrene and hydrogen peroxide gave a similar response to the uninhibited system (Supporting Information, Figure S5). Substitution at the 2 and 4 positions on imidazole has been shown to significantly reduce its interaction in the cyt P450 active site.[42] In comparison to imidazole-4-acetic acid and sulconazole, the combination of the 2 and 4 substituents negate any inhibitory effects.[42] The initial rates were calculated for each inhibitor using the sensor ratio (Table 1). The initial rates decreased with increased inhibitor concentration for each inhibitor. An illustration of these trends is shown for each inhibitor in Figure 3. These data were fitted with the Michaelis−Menten inhibition models to determine the inhibition constants.

To ensure that imidazoles were directly inhibiting cyt P450cam, incubations of styrene, inhibitors, and cyt P450cam were conducted in the absence of DNA. Films of cyt P450cam and PDDA were generated on silica nanospheres to form biocolloid reactors. The biocolloid reactors were incubated with styrene, hydrogen peroxide, with and without 500 μM inhibitors followed by liquid chromatographic analysis. Liquid chromatography analysis of styrene oxide formation was conducted for 10 min incubation time at 37 °C. A comparison of the percent inhibition versus the uninhibited control (Styrene and hydrogen peroxide only) was

Table 1. Initial Rates of Inhibition As Determined from Sensor Ratio Plots at Each Concentration of Inhibitor

inhibitor	imidazole		imidazole-4-acetic acid		sulconazole	
μM	v_o[a]	R^2[b]	v_o	R^2	v_o	R^2
0	0.142 ± 0.013	0.98				
50	0.138 ± 0.011	0.99	0.121 ± 0.013	0.98	0.101 ± 0.023	0.82
100	0.113 ± 0.013	0.72	0.096 ± 0.007	0.93	0.090 ± 0.006	0.96
150	0.107 ± 0.029	0.91	0.085 ± 0.009	0.99	0.082 ± 0.023	0.83
250	0.092 ± 0.015	0.99	0.059 ± 0.023	0.95	0.082 ± 0.003	0.89
500	0.081 ± 0.0157	0.98	0.057 ± 0.002	0.85	0.036 ± 0.002	0.56

[a] v_o is the initial rate. [b] R^2 is the correlation coefficient linear fits of initial rate.

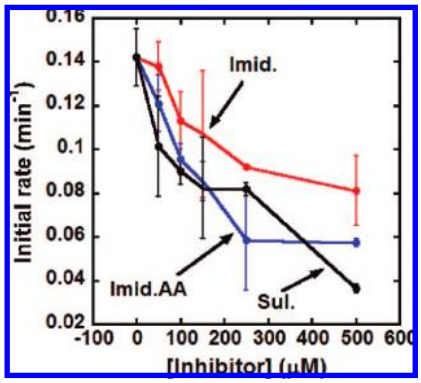

Figure 3. Inhibitor concentration versus initial rates for imidazole (Imid.), imidazole-4-acetic acid (Imid.AA), and sulconazole (Sul.) as determined from SWV sensor ratios. Error bars (standard deviations for $n = 3$) are included for every initial rate.

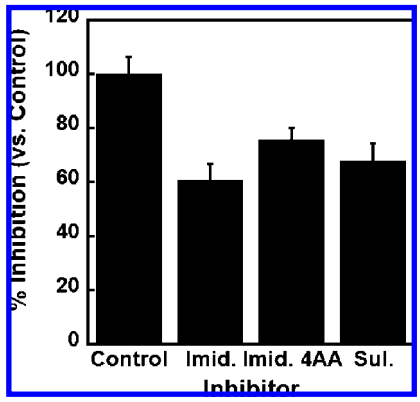

Figure 4. Inhibition of cyt P450cam metabolism of styrene using imidazole inhibitors in the absence of DNA on biocolloid nanoreactors. Liquid chromatographic responses observed for styrene, hydrogen peroxide, with and without 500 μM inhibitor. Signals expressed as percentage of control (no inhibitor) after 10 min incubation at 37 °C. Abbreviations: Imidazole (Imid.), imidazole-4-acetic acid (Imid.4AA), and sulconazole (Sul.) were used in the inhibition.

generated (Figure 4). Signals attributed to styrene metabolism reduced after 10 min of incubation with 500 μM of each inhibitor. This ensured that inhibition of DNA damage was occurring in our enzyme/DNA biosensor because of inhibitor interactions with the enzyme active site.

Evaluation of Michaelis−Menten Constant (K_m*). In order determine the Michaelis−Menten inhibition constants, an apparent Michaelis−Menten dissociation constant (K_m*) was needed. To evaluate K_m*, sensor signals were determined as a function of the amount of styrene (v/v) at 0.05% (4.35 mM), 0.10% (8.70 mM), 0.15% (13.05 mM), 0.25% (21.75 mM), and 0.5% (43.5 mM). The noted concentrations are the dispersed concentrations of styrene ($C_{disp.}$). The sensor ratio (Ip_F/Ip_I) versus incubation time at each % styrene is shown in Figure 5A. The sensor ratios increased with increasing styrene concentration initially, followed by a leveling at high concentration. The Michaelis−Menten equation was used to fit the nonlinear plot yielding values of apparent K_m* and V_m* (Figure 5B). Additionally, a double reciprocal plot (Lineweaver−Burk plot) of initial rate and styrene concentration allowed extrapolation of K_m* ($-x$ intercept) and V_m* (y intercept, Figure 5C) as is shown. The nonlinear fit of the Michaelis−Menten equation yielded a K_m* of 2.6 ± 0.5 mM and a V_m* of 0.176 ± 0.006 min^{-1} for styrene. The values extrapolated from the double reciprocal plot for K_m* and V_m*, 3.0 mM and 0.182 min^{-1}, respectively, were in good agreement. The determined Michaelis−Menten constant is indicative of the cyt P450cam metabolism of styrene as detected from the electrochemical signal that arises because of styrene oxide DNA damage. The apparent Michaelis−Menten constant and maximal velocity (rate, V_m) was used in nonlinear fits to evaluate inhibition constants.

Evaluation of Michaelis−Menten Inhibition Constants. Using the estimated K_m* and V_m* for the biosensor, the Michaelis−Menten inhibition models (eqs 3−7) were used to approximate inhibition constants (with the exception of applying the simple competitive model with and without V_m*). To achieve this, the initial rates versus concentration trends were fitted using the competitive, uncompetitive, and noncompetitive inhibition models (eqs 3−7). The data were evaluated using the graphical program KaleidaGraph, with an initial estimated value of the unknown parameter (K_I*, 100 μM) followed by nonlinear regression fitting. The apparent Michaelis−Menten constant, maximal velocity, and styrene concentration were also employed as constants for fitting. After convergence, a value of the inhibition constant was displayed along with a correlation coefficient and χ^2 (chi squared). Examples of fits using the uncompetitive and simple competitive (without V_m*) models for imidazole, imidazole-4-acetic acid, and sulconazole are shown in Figure 6 and 7, respectively (see Supporting Information, Figures S7−S9 for additional fits of inhibition models). The corresponding values of K_I* from the uncompetitive, simple competitive fits, and selected inhibition models are shown in Table 2 (see Supporting Information, Table S1 for the complete table). Attempts of nonlinear fits using the competitive (eq 3) and noncompetitive (eq 5) models yield unstable values of the apparent inhibition constant. In the case of the competitive inhibition model, the correlation coefficient and apparent inhibition constant were negative. Fits with the noncompetitive model yielded values of

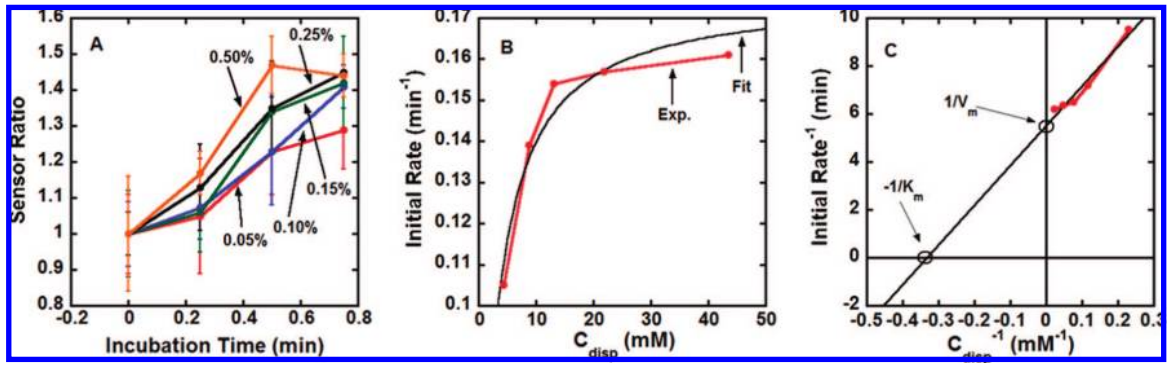

Figure 5. Evaluation of apparent Michaelis−Menten constant (K_m*) using initial rates of DNA damage obtained from the slopes of sensor ratios at various styrene concentrations. Sensor ratios determined from SWV of (PDDA/DNA/CYP101/)$_2$ PDDA/DNA films in 50 mM NaH_2PO_4 pH 7.0/50 mM NaCl with 50 μM $Ru(bpy)_3Cl_2$. (A) Ratio currents versus incubation time as a function of styrene concentration. (B) Michaelis−Menten nonlinear fit to initial rates versus styrene concentration. (C) Lineweaver−Burk plot used in secondary analysis of K_m*.

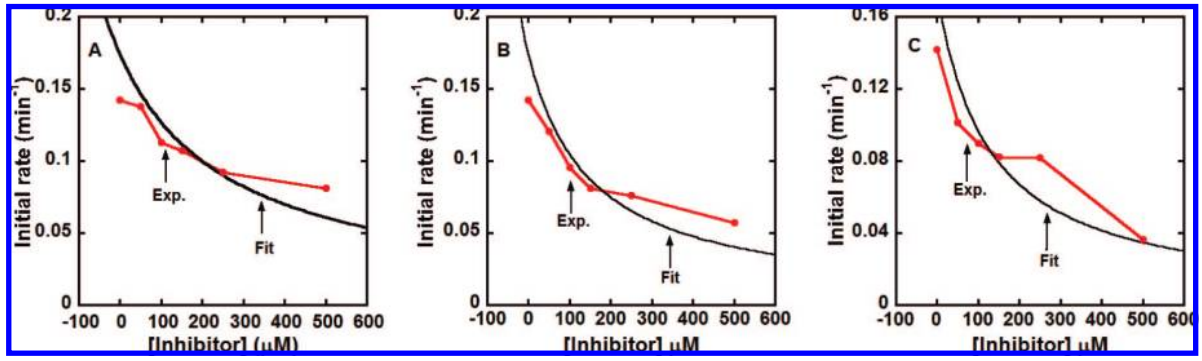

Figure 6. Nonlinear fits using the uncompetitive model (eq 4) to determine the apparent K_I'' for imidazole (A), imidazole-4-acetic acid (B), and sulconazole(C). The apparent K_m and V_m values were used for these nonlinear fits. An estimated K_I value of 100 μM was used as starting point for iteration.

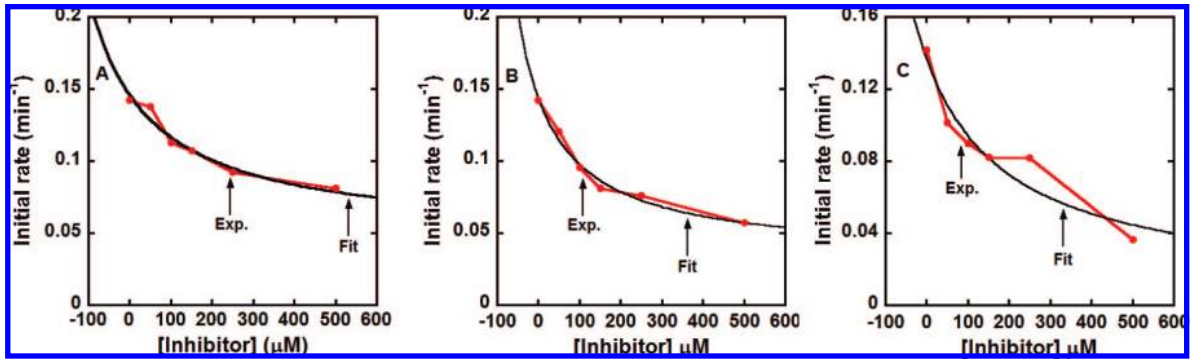

Figure 7. Nonlinear fits using the simple competitive (no estimated values, eq 6) model to determine the apparent K_I'' for imidazole (A), imidazole-4-acetic acid (B), and sulconazole (C). The apparent K_m and V_m values were used in these nonlinear fits as predetermined constants. An estimated K_I value of 100 μM was used as starting point for iteration.

the apparent inhibition constant that were either unusually large or negative, indicating, an inability to approximate the inhibition trends.

Results of the nonlinear fits were compared to the Michaelis−Menten inhibition models that were linearized by taking the double reciprocal (Lineweaver−Burk).[53] The inhibition data were plotted as the inverse of initial rate (v^{-1}, min) versus inhibitor concentration (Dixon Linear plot).[56,57] The apparent inhibition constants were determined by fitting the linearized inhibition model to the Dixon plots for imidazole, imidazole-4-acetic acid, and sulconazole. The apparent K_I* determined are shown in Table 2. The noncompetitive models yielded unstable apparent inhibition constants in a similar fashion as the nonlinear fits. While the values of K_I* were evaluated from fits of various inhibition models, the mechanism of inhibition remained unclear. To correctly assess the appropriate inhibition mechanism, goodness of fit criteria were employed.

Goodness of fit criteria were used to determine how well the mathematical expressions approximated measured values. The

(56) Dixon, M. *Biochem. J.* **1953**, *55*, 170–171.
(57) Cortes, A.; Cascante, M.; Cardenas, M. L.; Cornish-Bowden, A. *Biochem. J.* **2001**, *357*, 263–268.

Table 2. Values of Inhibition Constants As Obtained from Linear and Nonlinear Fits Using the Various Inhibition Mechanisms[a]

		imidazole		imidazole-4-acetic acid		sulconazole	
model	P[d]	value	R^2	value	R^2	value	R^2
uncomp.	K_I*′	268.2 ± 59.8	0.44	149.8 ± 31.4	0.67	124.0 ± 30.1	0.64
simple comp. (val.)	K_I* [b] V_1 [c]	89.5 ± 66.35 0.06 ± 0.03	0.61	67.3 ± 42.1 0.04 ± 0.02	0.75	58.1 ± 44.7 0.04 ± 0.03	0.68
simple comp.	K_I* V_m [c] V_1	245.0 ± 139.3 0.15 ± 0.01 0.05 ± 0.02	0.96	142.3 ± 4.5 0.14 ± 0.01 0.03 ± 0.01	0.98	204.2 ± 154.2 0.14 ± 0.01 0.01 ± 0.04	0.92
DLU	K_I*′	360.0 ± 51.6	0.58	213.3 ± 25.1	0.76	139.0 ± 12.5	0.91

[a] See full table in Supporting Information, Table S1. All cases except the simple competitive mechanism (no estimated values) employed both the apparent K_m* and V_m*. [b] In units of micromolar. [c] V_m, V_1 (in units of min^{-1}). [d] Unknown parameter (*P*) evaluated by fitting. V_1 in the simple competitive mechanisms is the maximal velocity associated with enzyme−inhibitor complex.[54] Abbreviations: Comp. (Competitive, eq 3), Uncomp. (Uncompetitive, eq 4), DLC (Dixon linear competitive, linearized eq 3), DLU (Dixon linear Uncompetitive, linearized eq 4), Comp. K_m^{-1} (rearranged competitive model caused by division of K_m, eq 7), Simple Comp. (Simple competitive model eq 6).

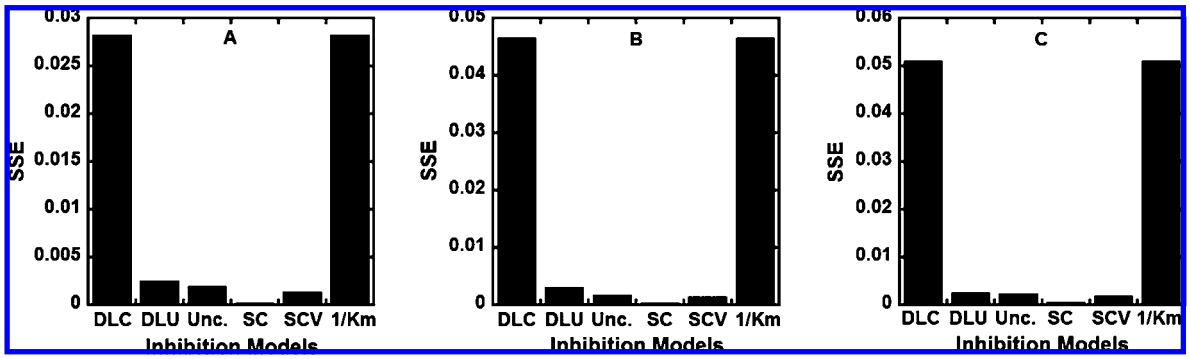

Figure 8. Sum of the squares of the errors (SSE) obtained using measured and calculated initial rates for each inhibitor. Calculated initial rates determine for each inhibition mechanism and resultant apparent inhibition constant. (A) Imidazole, (B)Imidazole-4-acetic acid, (C) Sulconazole. Abbreviations: DLC (Dixon linear competitive), DLU (Dixon linear Uncompetitive), Unc. (Uncompetitive), SC (Simple Competitive), SCV (Simple Competitive with estimated maximal velocity), and 1/K_m (Competitive 1/K_m rearrangement).

criteria included the analysis of correlation coefficients (R^2), and the evaluation of the sum of the squares of the errors (SSE). The correlation coefficient (R^2) was the initial diagnostic of how well a specific inhibition model fits the data. The best R^2 values were obtained with the simple competitive inhibition with no estimated values in the nonlinear fit (Table 2). On the basis of R^2, the simple competitive model (no V_m*) gave the best approximations of apparent K_I* for each inhibitor. However, while the correlation coefficients from the competitive and uncompetitive linear fits were poor for imidazole and imidazole-4-acetic acid, for sulconazole the R^2 values for those two mechanisms were similar to the value obtained for simple competitive model (no estimated values). Using the correlation coefficient as the initial goodness of fit criteria, while apparently successful for imidazole and imidazole-4-acetic acid, was inconclusive in determining the correct mechanism for sulconazole. Therefore, additional goodness of fit criteria were needed to properly discern the correct model of inhibition.

Additional goodness of fit criteria were evaluated by generating a comparison of the calculated model versus experimentally measured data. Using the calculated and experimentally measured initial rates, a sum of the square of the errors (SSE) analysis was undertaken.[54] As described in the Experimental Section, SSE is calculated by taking the difference between measured and calculated values, squared, and summed. The lowest value of SSE as determined for each inhibition mechanism represents the best model for a given inhibitor. SSE values calculated for each inhibition mechanism and inhibitor are graphically displayed in Figure 8. The simple competitive model (SC, no V_m* in the fit) yielded the lowest SSE values for each inhibitor. Using the SSE analysis, the best fitting method for imidazole, imidazole-4-acetic acid, and sulconazole was the simple competitive model (eq 6, no V_m*). The other inhibition methods had higher SSE values, and the calculated initial rates were not as good an approximation of the measured values. Using the goodness of fit criteria, we concluded that the simple competitive model (eq 6) was the mechanism of inhibition occurring in our enzyme/DNA biosensor, and the respective apparent inhibition constant represents the magnitude of inhibition for imidazole, imidazole-4-acetic acid, and sulconazole. Furthermore, the best inhibitor was imidazole-4-acetic acid because of a low K_I* relative to the other inhibitors.

DISCUSSION

Results presented above showed that enzyme/DNA biosensors with catalytic voltammetric detection are effective tools for rapid quantitative investigation of cyt P450 enzyme inhibition. As expected, sensor results showed that imidazole, imidazole-4-acetic acid, and sulconazole efficiently inhibited DNA damage that was facilitated by cyt P450cam metabolism of styrene to its genotoxic

product styrene oxide. The signal-to-noise of the sensor response was sufficient to allow the evaluation of Michaelis−Menten inhibition models to extract apparent inhibition constants. In the absence of inhibitors, the DNA damage signals increased with incubation time indicating cyt P450cam metabolism of styrene to styrene oxide and concurrent styrene oxide-DNA adduct formation (Figure 1A,B), as reported previously.[19,22,28,29] Control experiments with styrene only and hydrogen peroxide only showed no increase in sensor ratios with incubation time, indicating no styrene oxide production without the initiator, and no contribution of hydrogen peroxide to observed signals (Figure 1B). The robust DNA damage signal obtained from the sensor was integral for monitoring changes in the presence of inhibitors.

For all inhibitors, increasing the inhibitor concentration caused a decreased DNA damage signal (Figure 2). The corresponding initial rates taken from the sensor ratio slopes for each inhibitor decreased with increased concentration (Figure 3). The observed changes in the DNA damage signal were in good agreement with previous reports.[21,32] Furthermore, liquid chromatography experiments with styrene, 500 μM inhibitors, and cyt P450cam in biocolloidal films confirmed inhibition of styrene oxide production (Figure 4). Control experiments conducted with only inhibitors had no increase in sensor ratios with respect to background (Supporting Information, Figure S6). This indicated that electrochemical signals were not impacted by the addition of inhibitors. The observed decrease in initial rates therefore was directly related to inhibition by imidazole, imidazole-4-acetic acid, and sulconazole.

Imidazoles have two chemical modes of inhibition. First, the N3 position in the ring can interact with the iron heme in cytochrome P450 isozymes.[37−40] Imidazole, for example, has a binding constant of 7.5 μM with cyt P450cam.[37] The imidazole binding interaction spectroscopically appears as a red shift cyt P450cam Soret band, representative of a shift from water bound to imidazole bound states.[37,39] This affinity for the cytochrome P450 active sites was a key component in imidazole inhibition, affecting heme reduction as well as oxygen binding. Second, imidazoles are capable of exerting antioxidant activity by quenching reactive oxygen species (ROS).[41−46] Reports have demonstrated the ability of imidazoles to scavenge singlet oxygen, hydroxyl radicals, and nitric oxide species. In the current system the metabolite styrene oxide is considered to be a ROS whose DNA damage has been reduced in presence of flavinoids and vitamin C.[21] Styrene oxide has been shown to react with imidazole and the histidine residue in proteins.[58,59] Therefore the inhibitors can exert bifunctional inhibition (CYP binding and/or styrene oxide scavenging) of DNA damage in our biosensor. The control experiment with 4-methyl-2-phenylimidazole showed no significant inhibitory effects (Supporting Information, Figure S5). This result was rationalized as a significant reduction in cyt P450 active site interaction (due 2 and 4 substituents on imidazole[42]) and reduction of antioxidant effect because of steric clashes with styrene oxide.

We successfully demonstrated the inhibition of DNA damage using our enzyme/DNA biosensor. Sensor ratios decreased with increased inhibitor concentration signifying the inhibitory effect. Using the inhibition trends (Figure 5) we evaluated apparent inhibition constants (K_I*) for each inhibitor by employing the predetermined values of Michaelis−Menten dissociation constant (K_m*) and maximal velocity (V_m*) in fits of each inhibition model (eq 3−7). Representative fits of the uncompetitive (eq 4, Figure 6) and the simple competitive (no values, eq 6, Figure 7) demonstrates how the values of K_I* arose (Table 2). The magnitude of the K_I* indicates the level of dissociation for each inhibitor in the presence of enzyme and substrate. The smaller the value of K_I* the less dissociation occurs indicating good inhibition. By this standard the lowest K_I* indicates the best inhibitor and the appropriate mode of inhibition. However, since regression analyses were used to evaluate K_I* then the goodness of fit of each inhibition model to the actual inhibition trends dictates the proper mechanism of inhibition and concurrently, the magnitude of the inhibition constant. Therefore, the values of K_I* (Table 2) by themselves do not yield any critical information in this analysis. To properly elucidate the appropriate inhibition model, and hence K_I*, goodness of fit analyses were undertaken. The goodness of fit criteria employed were a comparison of correlation coefficients (R^2) and a sum of the square of the errors analysis (SSE).

The correlation coefficients (R^2, Table 2) reflect how well a fit (linear or nonlinear) approximates the data. The values are typically internally determined when employing fits in graphical programs. The closer R^2 is to unity the better the fit of an equation to the data. Of the values listed (Table 2), the simple competitive model (no estimated values) yielded the best R^2 for all inhibitors with the exception of linearized competitive and uncompetitive models for sulconazole. At this juncture we could have concluded that the simple competitive method was the mode of inhibition for these inhibitors; however, the conflict that arose with sulconazole suggested that R^2, by itself, was not the best diagnostic of the inhibition mechanism.

We then turned to the sum of the squares of the errors (SSE) to ascertain the mode of inhibition. SSE analysis calculates the difference between measured and calculated values (initial rates as calculated with K_I* determined from fits) followed by squaring of each difference and then finally the summation of all squared differences. From evaluating SSE for the inhibition models employed in fits, the simple competitive model had the lowest SSE for each inhibitor indicating that it was the best fit (Figure 8). Of all the inhibition models, the simple competitive model (no estimated value) gave calculated initial rates similar to the experimentally measured initial rates. Combining the goodness of fit criteria, we established that the simple competitive model (no estimated values) and corresponding K_I* values represented the mode of inhibition for imidazole, imidazole-4-acetic acid, and sulconazole as observed with our enzyme/DNA biosensor. Therefore, the inhibitors competed with the styrene substrate for cyt P450cam active site and/or acted as antioxidant toward styrene oxide causing a reduction in the amount of DNA damage signals observed.

In summary, using electrochemical DNA-cyt P450 sensors, we observed inhibition of DNA damage using imidazole inhibitors (imidazole, imidazole-4-acetic acid, and sulconazole) and evaluated inhibition constants for each inhibitor. We demonstrated through goodness of fit criteria that these inhibitors act via a simple

(58) Torregrosa, R.; Pastor, I. M.; Yus, M. *Tetrahedron* **2007**, *63*, 469–473.
(59) Kaur, S.; Hollander, D.; Haas, R.; Burlingame, A. L. *J. Biol. Chem.* **1989**, *264*, 16981–16984.

competitive mechanism. The inhibitors competed with styrene for the enzyme active site and/or competed with DNA damage sites for interaction with styrene oxide. Of the inhibitors used, imidazole-4-acetic acid exhibited the lowest K_I*; therefore, it was the best inhibitor in our system. These model inhibition experiments allow the use of enzyme/DNA sensors as rapid screening tools for drug-drug interactions of pharmaceutical candidates.

ACKNOWLEDGMENT

This work was supported financially by U.S. PHS grant ES03154 from the National Institute of Environmental Health Sciences (NIEHS), NIH.

SUPPORTING INFORMATION AVAILABLE

Additional experimental methods and nine supplementary figures detailing sensor film formation monitored by quartz crystal microbalance, square wave voltammograms at each inhibitor concentration, control 4-methyl-2-phenylimidazole sensor response, sensor signals for inhibitor controls, a complete table of inhibition constants evaluated for each inhibition model, and addition fits of Michaelis−Menten inhibition models are shown. This material is available free of charge via the Internet at http://pubs.acs.org.

Received for review October 14, 2008. Accepted November 23, 2008.

AC802179S